Bioactive Materials 5 (2020) 709–720

Contents lists available at ScienceDirect

Bioactive Materials

journal homepage: http://www.keaipublishing.com/biomat

Antibacterial and cytocompatible coatings based on poly(adipic anhydride) for a Ti alloy surface

Katarzyna Leśniak-Ziółkowska[a], Monika Śmiga-Matuszowicz[b], Agata Blacha-Grzechnik[b], Sebastian Student[c,d], Monika Brzychczy-Włoch[e], Małgorzata Krok-Borkowicz[f], Elżbieta Pamuła[f], Wojciech Simka[a], Alicja Kazek-Kęsik[a,c,*]

[a] Faculty of Chemistry, Silesian University of Technology, B. Krzywoustego Street 6, 44-100, Gliwice, Poland
[b] Faculty of Chemistry, Silesian University of Technology, M. Strzody 9 Street, 44-100, Gliwice, Poland
[c] Biotechnology Centre, Silesian University of Technology, B. Krzywoustego 8 Street, 44-100, Gliwice, Poland
[d] Department of Systems Biology and Engineering, Faculty of Automatic Control, Electronics and Computer Science, Silesian University of Technology, Akademicka 16 Street, 44-100, Gliwice, Poland
[e] Department of Microbiology, Jagiellonian University Medical College, Czysta 18 Street, 31-121, Krakow, Poland
[f] Faculty of Materials Science and Ceramics, AGH University of Science and Technology, Mickiewicza Av. 30, 30-059, Krakow, Poland

ARTICLE INFO

Keywords:
Titanium alloy
poly(adipic anhydride)
Antibacterial coatings
Cytocompatible
Dental implants

ABSTRACT

This paper describes a formation of hybrid coatings on a Ti–2Ta–3Zr–36Nb surface. This is accomplished by plasma electrolytic oxidation and a dip-coating technique with poly(adipic anhydride) (($C_6H_8O_3$)n) that is loaded with drugs: amoxicillin ($C_{16}H_{19}N_3O_5S$), cefazolin ($C_{14}H_{14}N_8O_4S_3$) or vancomycin ($C_{66}H_{75}Cl_2N_9O_{24}$ · xHCl). The characteristic microstructure of the polymer was evaluated using scanning electron microscopy and confocal microscopy. Depending on the surface treatment, the surface roughness varied (between 1.53 μm and 2.06 μm), and the wettability was change with the over of time. X-ray photoelectron spectroscopy analysis showed that the oxide layer did not affect the polymer layer or loaded drugs. However, the drugs lose their stability in a phosphate-buffered saline solution after 6.5 h of exposure, and its decrease was greater than 7% (HPLC analysis). The stability, drug release and concentration of the drug loaded into the material were precisely analyzed by high-performance liquid chromatography. The results correlated with the degradation of the polymer in which the addition of drugs caused the percent of degraded polymer to be between 35.5% and 49.4% after 1 h of material immersion, depending on the mass of the loaded drug and various biological responses that were obtained. However, all of the coatings were cytocompatible with MG-63 osteoblast-like cells. The drug concentrations released from the coatings were sufficient to inhibit adhesion of reference and clinical bacterial strains (*S. aureus*). The coatings with amoxicillin showed the best results in the bacterial inhibition zone, whereas coatings with cefazolin inhibited adhesion of the above bacteria on the surface.

1. Introduction

Implantology is a field of science that is constantly developing due to an increasing number of biomaterials. Although a wide range of biomaterials is known, titanium and titanium alloys have found widespread use in implantology, for example, in orthodontic surgery. Currently, a titanium Grade 4 and Ti–6Al–4V alloy is the most popular biomaterial in orthopedic and orthodontic implant areas. Titanium implants might be used for soft tissue and for hard, bone tissue, as well. Due to their good mechanical properties, biocompatibility and corrosion resistance in simulated body fluid, titanium alloys are often used compared to the Co–Cr or stainless steel implants [1–3]. Vanadium, being a part of the Ti–6Al–4V alloy, is hazardous to human health due to the toxicity of its corrosion products. A vanadium corrosion product, such as V_2O_5, can lead to disorders of the cardiovascular system, heart and kidneys, as well as Parkinson's disease [4]. Additionally, aluminum compounds and aluminum ions have a negative effect on human organisms because their ions can be released and accumulated in the brain, leading to diseases of the nervous system [5,6]. These problems increase the intensity of research on vanadium-free and aluminum-free titanium biomaterials. An innovative titanium alloy is a Ti–23Nb-0.7Ta–2Zr-1.2 alloy, also known as Gum Metal, due to its low Young's

Peer review under responsibility of KeAi Communications Co., Ltd.
* Corresponding author. Faculty of Chemistry, Silesian University of Technology, B. Krzywoustego Street 6, 44-100, Gliwice, Poland.
E-mail address: alicja.kazek-kesik@polsl.pl (A. Kazek-Kęsik).

https://doi.org/10.1016/j.bioactmat.2020.04.020
Received 22 January 2020; Received in revised form 21 April 2020; Accepted 27 April 2020

modulus and specific plastic properties that cause it to be flexible [7]. This alloy is a promising material without aluminum and vanadium compounds and shows good mechanical properties, such as high elasticity, plasticity and strength, which are desirable for long-term bone tissue implants. The Young's modulus of Gum Metal (~40 GPa) is also lower than Ti–6Al–4V (~110 GPa), which results in better adjustment to the Young's modulus of bone [8,9].

To obtain high biocompatible and cytocompatible properties of the biomaterials, a surface modification of the titanium alloys might be an easy solution. The plasma electrolytic oxidation (PEO) process is widely used for the formation of functional coatings on titanium alloy surfaces. During the PEO process, glow discharge and plasma occurs when the oxide layer breaks down and the electric field accumulates near the electrode surface and released gas [10]. Due to the anodization process, a layer formed on the metal surface may increase its corrosion resistance in simulated body fluid [11]. One of the important advantages of the PEO process is that during anodizing, the elements and compounds from the anodizing bath may be incorporated into the layer [12]. For example, the incorporation of calcium and its compounds into the TiO_2 layer may support the adhesion of osteoblast cells, and their proliferation provides for improved osseointegration processes [13]. Additionally, relatively simple voltage and current density control allows the formation of oxide layers with controlled porosity [10].

After dental implantation, inflammation always occurs due to soft and hard tissue damage. However, septic inflammation may occur causing the loss of implants or promoting bone disease. Septic bone disease, called osteomyelitis, is a dangerous illness that not only is painful and problematic but also has long-term treatment which may provide to remove the implant. The most common bacterial pathogens causing osteomyelitis are *Staphylococcus aureus, Staphylococcus epidermidis, Pseudomonas aeruginosa* and *Escherichia coli* [14–16]. As a consequence of bone inflammation, bone and tissue necrosis and destruction appear. A detailed mechanism of osteomyelitis progress is presented in the literature [17]. Due to these risks, patients need to be treated with specifically selected antibacterial agents, which also influence other parts of the human or animal [18]. The most common method of dosing antibiotics is the conventional oral route. A large dose of antibiotics must be delivered once, and it can be up to 1.5 g per day, using amoxicillin as an example [19]. There are some disadvantages for using large doses of drugs, e.g., a large possibility of side effects and allergic reactions and the necessity for taking frequent and high doses of the drug. Metabolic drugs may sometimes accumulate in organisms, and these drugs have been detected in high concentrations in the environment due to organism waste. The high concentrations of antibiotics and the periods of patient treatment by antibiotics also cause several problems with antibiotic-resistant microbes, which are often discussed worldwide. These troubles have resulted in the search for new, safer and more convenient routes of drug delivery – implant drug delivery system (IDDS) [20]. Incorporation of drugs into an implant can resolve the above problems and initiate some improvements. To obtain such an effect, biodegradable polymers can be used [21,22].

Thus far, biodegradable polymers such as poly(lactic-acid) (PLA), poly(glycolic acid) (PGA), poly(ϵ-caprolactone) (PCL) and poly(lactide-co-glycolide) (PLGA) are well known and widely used is used as biomaterials in the field of bone tissue engineering [22–24]. The combination of titanium oxide layers obtained by the PEO process with biodegradable polymers allows the design of innovative hybrid oxide-polymer coatings [25]. In drug delivery systems, biodegradable polymers can be a matrix for releasing drugs. Depending on the polymer, the drug release kinetics are different. In the case of applying biodegradable matrices, the drug can be delivered directly to an infected place with a controlled time of release. Due to greater precision of the drug delivery method, the necessary drug concentration is smaller, and as a result, the number of side effects decrease [26]. Because antibiotics have often been taken in high doses, bacteria in recent years have increased their ability to withstand antibiotics. Using small doses of drugs, e.g., IDDS, may slow down this process [27].

Among the biodegradable polymers, poly(adipic anhydride) (PADA) seems to be an interesting choice for IDDS application. This polymer distinguishes itself from others with its fast degradation ability (approximately 24 h depending on degradation conditions) [28,29]. Due to its fast degradation (depending on pH, it is usually up to several hours) and nontoxic hydrolysis products, PADA is considered a strong candidate for polymer matrices used in IDDS [30,31]. Additionally, there are some difficulties related to the effectiveness of antibiotic incorporation into an implant surface layer. Drugs are characterized by limited stability over time. Depending on the chemical surroundings of the antibiotics, they can degrade due to changes to their active chemical structure becoming ineffective against bacteria. For this reason, having a short for polymer matrix degradation and drug release time provides a strong possibility of an observable antibacterial effect.

The aim of this work was to obtain hybrid layers consisting of titanium porous oxide and a PADA layer loaded with selected drugs such as amoxicillin, cefazolin or vancomycin. The surface of a Ti–2Ta–3Zr–36Nb alloy was anodized to form porous oxide layers at high voltage. The polymeric part of the coating was formed using a dip-coating method, and the appropriate conditions for forming functional coatings were found. The surface morphology, surface roughness, wettability, and chemical composition of the materials were analyzed and discussed. The polymer layer and layer loaded with drugs were analyzed using a confocal microscope. Drug concentrations released from the coatings and drug stabilities were precisely analyzed and determined by high-performance liquid chromatography. Antibacterial properties were evaluated using reference and clinical *Staphylococcus aureus* strains. Cytocompatibility was evaluated based on the metabolic activity of the osteoblast-like cell line MG-63. Optimal parameters for coating formation were found in order to obtain the best physicochemical properties of a material that would be desirable for dental implants.

2. Materials and methods

2.1. Titanium alloy surface treatment

Samples of titanium alloy were cut from a metal rod (Ti–2Ta–3Zr–36Nb, BIMO, Poland). The titanium alloy surfaces were polished using SiC abrasive papers with granulation up to 1000. Then, the pretreated titanium alloy samples were anodized in 0.1 M Ca $(H_2PO_2)_2$ solution at 300 V for 5 min. The current density during the process was 150 mA·cm^{-2}. The plasma electrolytic oxidation (PEO) process was carried out at 300 V and 150 mA·cm^{-2} for 5 min. The anodized samples were washed with deionized water and dried at room temperature. The PEO process was performed in a cooled electrolyzer; a Ti mesh was used as the cathode and the Ti alloys were used as the anode to modify their surfaces.

2.2. Synthesis of poly(adipic anhydride)

Poly(adipic anhydride) (PADA) was synthesized from adipic acid by a two-step acetylation and melt polycondensation method as reported in the literature [32]. In the first step, prepolymer was obtained by refluxing adipic acid in acetic anhydride (1:10 w/v) under a nitrogen atmosphere for 0.5 h. Excess acetic anhydride and acetic acid formed in this reaction as products and were removed with a rotary evaporator. The prepolymer was formed by acetylation and in the second step was condensed to yield PADA by heating at 150 °C for 2 h under high vacuum (0.1 mm Hg). The yield was approximately 70%. The obtained polymer was stored in a freezer before being used in further experiments without purification. The expected chemical structure of PADA was confirmed by ^{1}H NMR and ^{13}C NMR.

PADA ^{1}H NMR ($CDCl_3$, ppm) δ: 2.40–2.60 (m, -C**H**$_2$C(O)OC(O)-), 2.22 (s, C**H**$_3$C(O)OC(O)-), 1.65–1.80 (m, -C**H**$_2$CH$_2$C(O)OC(O)-).

Table 1
Sample labels of the titanium alloy surfaces.

sample label	PEO	dip-coating in 1% PADA solution	antibiotic in hybrid layer		
			amoxicillin	cefazolin	vancomycin
GM	×	×	×	×	×
GM-PEO	✓	×	×	×	×
GM-PADA	✓	✓	×	×	×
GM-PADA_AMX	✓	✓	✓	×	×
GM-PADA_CEF	✓	✓	×	✓	×
GM-PADA_VANCO	✓	✓	×	×	✓

PADA ^{13}C NMR ($CDCl_3$, ppm) δ: 168.84 (**C**=O), 34.69 (-**C**H_2C(O)OC(O)-), 23.26 (-**C**H_2CH_2C(O)OC(O)-). The average molecular weight of PADA was calculated from an integration of the ^1H NMR signals and equaled 15 980.

2.3. Formation of the hybrid oxide-PADA layer

To form polymer layers on the anodized surface of the titanium alloy (labeled GM), the sample was immersed in 1% (w/v) PADA solution in $CHCl_3$ (Sigma Aldrich, Poland) as a solvent. The samples were immersed in this solution at a speed of 0.2 cm·min^{-1}. The time of immersion in the PADA solution was 1 min for each one. Then, samples were removed from the solution and dried at room temperature. PADA layers loaded with drugs were prepared similarly, except that one of three different antibiotics (amoxicillin or cefazolin or vancomycin) was added to the polymer solution in an amount of 5 wt.% of the mass of PADA. Table 1 presents the sample labels of the titanium alloys after the surface treatment.

2.4. Surface analysis

The morphology of the PEO coatings and hybrid layers was investigated using a scanning electron microscope (Phenom Pro-X) with voltages up to 5 kV. 3D SEM images were taken, and the roughness of the surface was investigated by using software to determine the arithmetic roughness profile (Ra). The results are presented as an average of 5 various lines analyzed for each sample. The surface wettability was analyzed by measuring the water contact angle (goniometer DataPhysics, OCA 15 EC, Germany). For this measurement, 0.2 μL of deionized water was dropped on the investigated surfaces, and the contact angle was measured over time. Three measurements from three independent samples were collected and averaged.

The thickness of the oxide layer was determined using the same scanning electron microscope (Phenom Pro-X). The sample was placed into an epoxy-resin and ground using abrasive paper and diamond paste according to the procedures presented in our previous paper [33]. For the polymer layer morphology, a confocal microscopy analysis was performed. The samples were immersed in a solution composed of Syto 9 dye (Thermo Fisher) and phosphate-buffered saline (PBS) solution for 15 min. Imaging was performed using an Olympus FV 1000 confocal microscope with 40 × /NA 0.95 objectives. Z-stack images were generated using a 488-nm laser for FITC dye. 3D data sets were analyzed as volume rendered data sets using Imaris (custom software developed by Bitplane Scientific Software, Zurich, Switzerland).

2.5. Chemical composition of the hybrid layer

X-ray photoelectron spectroscopy (XPS) investigations were conducted using a PREVAC EA15 hemispherical electron energy analyzer with a 2D multichannel plate detector. The samples were irradiated an energy of 1486.6 eV provided by an Al-K_α X-ray source (PREVAC dual-anode XR-40B). The base pressure of the system was $5{\cdot}10^{-9}$ Pa. The following parameters were applied during spectra acquisition: for survey spectra, 200 eV pass energy and a 0.9-eV scanning step and for high-resolution spectra, 100 eV pass energy and a 0.05-eV scanning step. All spectra were taken with a normal take-off angle. The energy scale of the analyzer was calibrated to Au $4f_{7/2}$ (84.0 eV)[25] and fitted using CASA XPS® software. The Shirley function was used for background subtraction, while the components were represented by a product of Gaussian (70%) and Lorentzian (30%) lines.

2.6. Polymer degradation

The degradation of PADA was investigated using ^1H NMR spectroscopy (300 MHz spectrometer, UNITY-INOVA, Varian). A 2-ml solution of 1% PADA and 5 wt% antibiotic (amoxicillin, cefazolin or vancomycin) was prepared. As a solvent, artificial saliva (1.3 g·dm^{-3} $NaHCO_3$, 1.2 g·dm^{-3} KCl, 0.7 g·dm^{-3} NaCl, 0.33 g·dm^{-3} KSCN, 0.26 g·dm^{-3} Na_2HPO_4 and 0.13 g·dm^{-3} urea; pH = 7.4) was used. Prepared solutions were incubated at 37 °C with 60 rpm shaking. After 1 h, 2 h, 4 h, 6 h, 8 h, 10 h, 12 h, 24 h and 48 h of degradation, the solutions were frozen and lyophilized, dissolved in the mixture of deuterated solvents $CDCl_3$/DMSO (1:1 v/v) and analyzed via ^1H NMR spectroscopy.

2.7. Drug release and its stability

To determine the released drug concentration, an HPLC technique (Merck-Hitachi chromatograph, pump L7100, DAD L-4500A) was used. Fifteen samples, each with one hybrid layer, were immersed in 5 ml artificial saliva and incubated at 37 °C. After 0.5 h, 1 h, 2 h, 4 h, 6 h, 8 h and 10 h, 200 μL of solution with the released drug was collected, and then, the collected solutions were averaged with three independent 1 ml analysis samples. For amoxicillin and cefazolin analysis, an additional sample was collected after 5 h of hybrid layer degradation. Before HPLC analysis, the solution was filtered (nylon filter, 0.22-μm pore diameter). HPLC analysis was carried out using a TSK gel ODS-100 V column, 150 mm × 4.6 mm with a particle size of 5 μm (TOSOH BIOSCIENCE). The temperature during analysis was 22 °C. As a mobile phase, 0.05% CF_3COOH in water and acetonitrile solution (90:10 v/v) was used. For cefazolin analysis, a mobile phase consisting of 0.05% CF_3COOH in water and acetonitrile solution (80:20 v/v) and a DAD detector were used. For amoxicillin, the wavelength was set to 230 nm, while for cefazolin the wavelength was 270 nm and for vancomycin, the wavelength was 280 nm. The calibration curves for amoxicillin, cefazolin and vancomycin determination in the artificial saliva matrix were prepared via a procedure presented in our last work [34].

Studies on drug (amoxicillin, cefazolin, vancomycin) stability were conducted at three different concentrations selected to represent the range of concentrations in real samples and the linearity range of calibration curves. Drug model solutions were prepared in PBS with concentrations of 1 μg·mL^{-1}, 24 μg·mL^{-1} and 50 μg·mL^{-1}. Three parallel samples of a given concentration were prepared, and each sample was injected thrice. An analysis was performed immediately after preparation of the solution (time zero) and then after 6.5, 13, 22 and 29 h for amoxicillin; 7, 14, 21 and 28 h for cefazolin; and 6.5, 13 and 21 h for vancomycin. All samples were stored at room temperature. The selected time point differences for each drug were due to the different times required for chromatographic analysis of each drug.

2.8. Antimicrobial properties investigations

The microbial tests were carried out using reference *Staphylococcus aureus* ATCC 25923 and clinical *Staphylococcus aureus* MRSA 1030 bacterial strains. Before testing, the bacteria were cultured in a Tryptic Soy Broth (TSB) culture medium (Biocorp, Poland) at 37 °C for 18 h (incubator ES-20/60, Biosan). First, the inhibition zones of bacteria were determined. The bacteria (~10^6 CFU·mL^{-1}) were spread onto agar plates (Muller-Hinton agar, Diag-Med Poland). Then, a 5-mm hole

was cut out from the middle of the agar plate. Next, 100 μL of sample solution (collected after hybrid layer degradation) was placed into this hole. Agar plates were incubated at 37 °C for 24 h, after which, the inhibition zones were measured.

2.9. Bacterial adhesion

Bacterial adhesion tests were carried out using two different bacterial strains: reference *Staphylococcus aureus* (ATCC 25923) and clinical *Staphylococcus aureus* (MRSA 1030). Before testing, the bacteria inoculate was incubated for 18 h at 37 °C in 50 cm^3 of BactoTM Tryptic Soy Broth (TSB) (Becton Dickinson). Then, the investigated samples were placed into 24-well plates. On their surfaces, 1 mL of bacterial suspension (~$1{\cdot}10^8$ CFU·mL^{-1}) was added, and the samples were incubated at 37 °C for 4 h with shaking at 60 rpm. Then, the samples were gently washed with PBS solution (8.0 g·L^{-1} NaCl, 0.2 g·L^{-1} KCl, 1.44 g·L^{-1} Na_2HPO_4, 0.24 g·L^{-1} KH_2PO_4). To remove the adhered bacteria, the samples were placed into new 24-well plates and treated intensively with 1 mL of 0.25% trypsin. Then, 100 μL of the bacteria and trypsin solution were collected and mixed with 0.9% NaCl at concentrations of 1:1000, 1:10 000, and 1:100 000. One hundred microliters of the prepared solutions were spread on agar plates. The agar plates were incubated at 37 °C for 24 h. After that, the bacterial colonies were counted.

2.10. Cytocompatibility

To determine the cytocompatibility of the Gum Metal surfaces, MG-63 osteoblast-like cells were used for testing. The investigated sample surfaces without polymer layers were sterilized in steam at 134 °C and under 2.1 bar pressure (Bravo 21V, SiCan). The PADA and drug-loaded PADA surfaces were sterilized using a laminar equipped with a UV lamp for 30 min. Sterilized samples were placed into 24-well plates. On the surfaces, MG-63 osteoblast-like cells were seeded. The cell density in the suspension was 8000 cells per sample. The samples were incubated at 37 °C for 7 days under a 5% CO_2 atmosphere. After 24 h, 3 days and 7 days, 100 μL of Alamar Blue (In Vitro Toxicology Assay Kit, Resazurin based, Sigma-Aldrich) was added to the surface of each sample. The samples were incubated at 37 °C for 4 h. Then, 100 μL of solution from each well was collected and placed into a new, 96-well plate. The absorption of collected solutions was measured with a FLUOstar Omega microplate reader (BMG Labtech) and a “live/dead” test was carried out. The investigated material was incubated with 2 μL of propidium iodide (1 mg·mL^{-1}) and AM calcein (1 mg·mL^{-1}) for 30 min. The surface morphologies were determined using a Zeiss Axiovert 40 (Carl Zeiss, Germany) optical microscope. The live cells are visible as green, and the dead are red.

3. Results

3.1. Surface characterization of hybrid layers

The 2D and 3D SEM images of the investigated surfaces are presented in Fig. 1. Pores visible on images are the result of the PEO process. The average roughness coefficient (Ra) value of the untreated GM surface was 0.61 μm ± 0.02. After PEO treatment, the Ra of the anodized GM surface increased to 1.24 μm ± 0.35 for the GM-PEO surface. Formation of the polymer (PADA) layer on the previously anodized GM alloy caused that Ra slightly increased up to 1.29 μm ± 0.05. However, the morphology and the surface roughness value were not significant different compared with the only anodized sample. 2D and 3D SEM images of the GM-PADA sample are presented in supplementary materials. The significant differences were detected where the confocal microscopy was applied. The Ra values of GM surfaces with hybrid layers containing antibiotics were measured with values of 1.53 μm ± 0.26 for GM-PADA_AMX, 1.92 μm ± 0.28 for GM-PADA_VANCO, and 2.06 ± 0.36 μm for GM-PADA_CEF, which was the highest observed value.

Anodization of the GM surfaces caused an oxide layer to form with open and closed pores. Thus, there was variation in the layer thickness and the cracks that might be formed in the layer due to spark discharges. Fig. 2A presents the cross-section of the GM-PEO layer observed using the SEM microscope. The thickness of the formed oxide layer was between 8.54 μm and 11.20 μm. Fig. 2B–E presents 3D images of the polymer layer with and without drugs. The thickness of the polymer layer was determined using a confocal microscope after immersing the samples in a solution with SYTO 9 dye. The layers cannot be observed using the SEM microscope. For the GM-PEO-PADA, the determined layer thickness was 13.77 μm, for the GM-PADA_AMX, it was 10.22 μm, for the GM-PADA_CEF, it was 9.87 μm, and for the GM-PADA_VANCO, it was 10.34 μm.

Fig. 3 presents the dynamic contact angle changes of the investigated GM surfaces as a function of time. The contact angle of all investigated surfaces was less than 90°, so it can be concluded that all investigated samples are hydrophilic. The most hydrophilic surface was observed for the GM-PADA_VANCO surface. Its contact angle measured 39.51° at the maximum point, and the total time of water drop spreading was 69 s. Similar tendency was observed for the sample without drug: GM-PADA. In comparison, the GM-PADA_AMX and GM-PADA_CEF were also characterized by low contact angle, indicates hydrophilic surfaces. The contact angle determined for the GM-PADA_AMX was 63.02°, and for the GM-PADA_CEF, it was 51.24°, while their water drop spreading times were less than 100 s. The measurements were stopped, where the surfaces became highly hydrophilic and the contact angle could not be determined.

3.2. Chemical composition of the hybrid layers

The chemical structures of the resulting inorganic and organic layers were confirmed by XPS.

The survey spectra recorded for all materials are presented in Fig. 4. For all the samples, signals coming from alloys covered with an oxide layer, i.e., O 1s, Ti 2p, Nb 3d and Ta 4f, and from species coming from the electrooxidation medium, i.e., Ca 2p and P 2p can be observed at approximately 530, 459, 210, 26, 347 and 134 eV, respectively.

In the next step, high-resolution spectra were recorded for PEO, giving more details about the chemical structure of the oxide layer. As shown in Fig. 5a, in the case of Ti 2p, one component, Ti $2p_{3/2}$, with its spin-orbit splitting counterpart is observed at 457.2 eV, indicating that Ti_2O_3 oxide was formed. Similarly, the regions for the Nb 3d and Ta 4f (Fig. 5b and c) reveal one component together with a spin-orbit splitting addition, $Nb3d_{5/2}$ at 207.5 eV and $Ta4f_{7/2}$ at 25.8 eV, suggesting the presence of metal oxides at the highest oxidation state, i.e., N_2O_5 and Ta_2O_5. Importantly, no additional signals arising from unoxidized metals are observed, which confirms the integrity and continuity of the oxide layer. Next, as shown in Fig. 6a, the representative position of the Ti 2p signal recorded for the GM-PEO surface covered with the polymeric layer remained unchanged, which proves that no covalent linkage is formed between the PADA and alloy oxides. As already mentioned, both phosphorus and calcium are introduced into the oxide layer during the electrochemical oxidation process. The high-resolution XPS spectrum of the P 2p region reveals two close spin-orbit components, P $2p_{3/2}$ and P $2p_{1/2}$, at 133.8 and 134.7 eV, respectively, which are typical for metal phosphates. Finally, the decomposition of the C 1s high-resolution spectrum recorded for the bare inorganic layer reveals three signals with maxima at 284.5, 286.7 and 288.7 eV that can be assigned to C–C, C–O and C═O, respectively, from the adventitious carbon layer. The same components are present in the C 1s region of GM-PADA, although the relative intensity of the C–O and C═O components is significantly higher when compared to the C–C component, which confirms the presence of a deposited polymeric layer (see Fig. 7).

Further modification of PADA by the introduction of antibiotics into

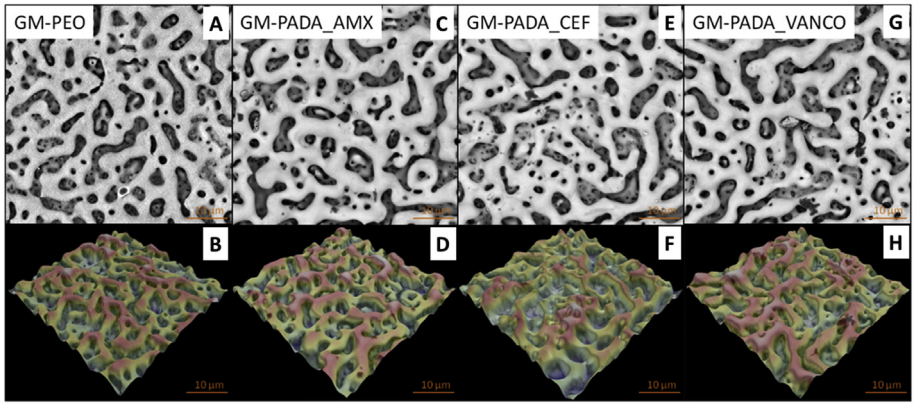

Fig. 1. 2D and 3D SEM images of the GM-PEO (A,B), GM-PADA_AMX (C,D), GM-PADA_CEF (E,F) and GM-PADA_VANCO (G,H) samples.

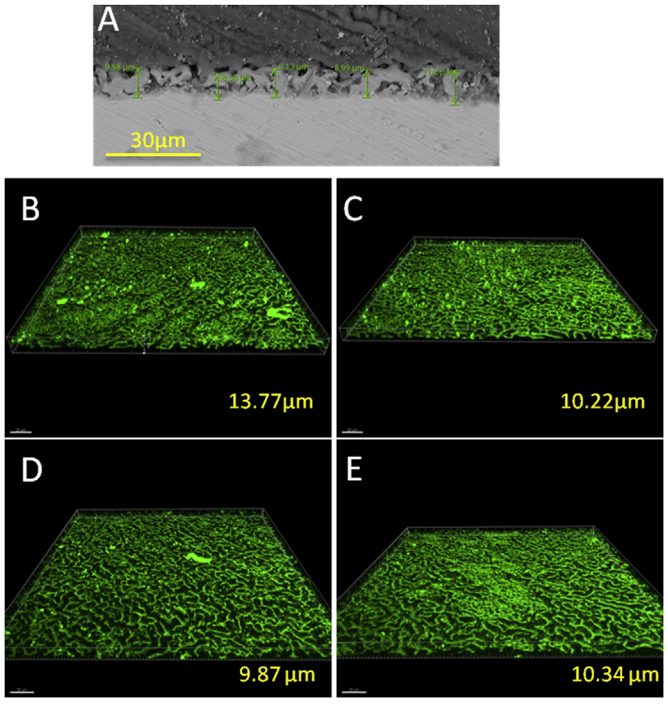

Fig. 2. SEM image of the cross-section for the GM-PEO sample (A) and the 3D images determined for the GM-PEO-PADA (B), GM-PADA_AMX (C), GM-PADA_CEF (D) and GM-PADA_VANCO (E) samples. The thickness of the anodized layer is between 8.54 and 11.20 µm. The thickness measurements of the polymer layers formed on the previously anodized surface of the titanium alloys are shown in the corner (yellow number). The addition of drugs influenced the polymer layer thickness, which significantly changed its biological activity.

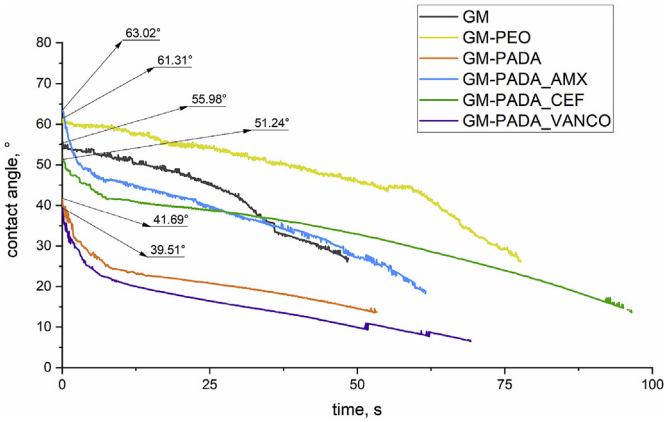

Fig. 3. Contact angle changes of the investigated surfaces as a function of time. The morphologies of the surfaces also significantly influenced the surface wettability and contact angle between the material and drop of water.

the polymeric matrix results in the appearance of additional N 1s signals at approximately 400 eV and S 2p signals at approximately 168 eV in the recorded survey spectra (Fig. 4) for GM-PADA_AMX and GM-PADA_CEF, and S 2p at approximately 168 eV for GM-PADA_VANCO. The high-resolution spectrum of S 2p (Fig. 6) acquired for GM-PADA_AMX shows two spin-orbit components with S $2p_{3/2}$ located at 166.0 eV, which can be assigned to the C–S bond. These results confirm that the active agents were successfully incorporated into the PADA polymer matrix.

3.3. PADA degradation

Table 2 presents the degradation of the polymer (PADA) and polymer with amoxicillin, cefazolin or vancomycin in various periods of time: 1 h, 2 h, 4 h, 6 h, 8 h, 10 h, 12 h, 24 h and 48 h.

Degradation progress is presented as the content of adipic acid groups, calculated as ratio of acid groups to sum of acid and anhydride groups. The hydrolysis percentage of the PADA polymer and the polymer with the drugs after 1 h of degradation is in the range from 35.5% for PADA_AMX to 49.4% for PADA_CEF. The results of ^{1}H NMR analysis of PADA hydrolysis progress indicate that the PADA polymer quickly degrades because over 50% of its initial mass is degraded after less than 12 h. In addition, based on the obtained results, it is worth noting that the degradation process depends on the kind of drug loaded into the polymer layer as degradation proceeded over 80% after 24 h. The PADA_AMX hybrid layer has the maximum hydrolysis percentage of 90.1% after 48 h.

3.4. Drug release concentration

Fig. 8 presents the results of the drug concentration after various exposure times of the drug in PBS solution.

The concentrations of amoxicillin, cefazolin and vancomycin were determined by HPLC after 6.5 h, 13 h, 20 h and 27 h of drug exposure in the vials. The concentrations of all the drugs significantly influenced their stability in PBS solution to optimize time for drug release from the hybrid coatings. After 6.5 h, prepared solutions with drug concentrations of 1 µg·mL^{-1} showed a decrease in stability by approximately 8%. The drugs showed much better stability in PBS solution when the drug concentrations were 25 µg·mL^{-1} or 50 µg·mL^{-1}. Vancomycin at a concentration of 1 µg·mL^{-1} was less stable in the PBS solution compared with the results determined for amoxicillin and cefazolin. When the concentration of drug in the PBS solution was 25 µg·mL^{-1}, vancomycin showed better stability, whereas the stability of amoxicillin

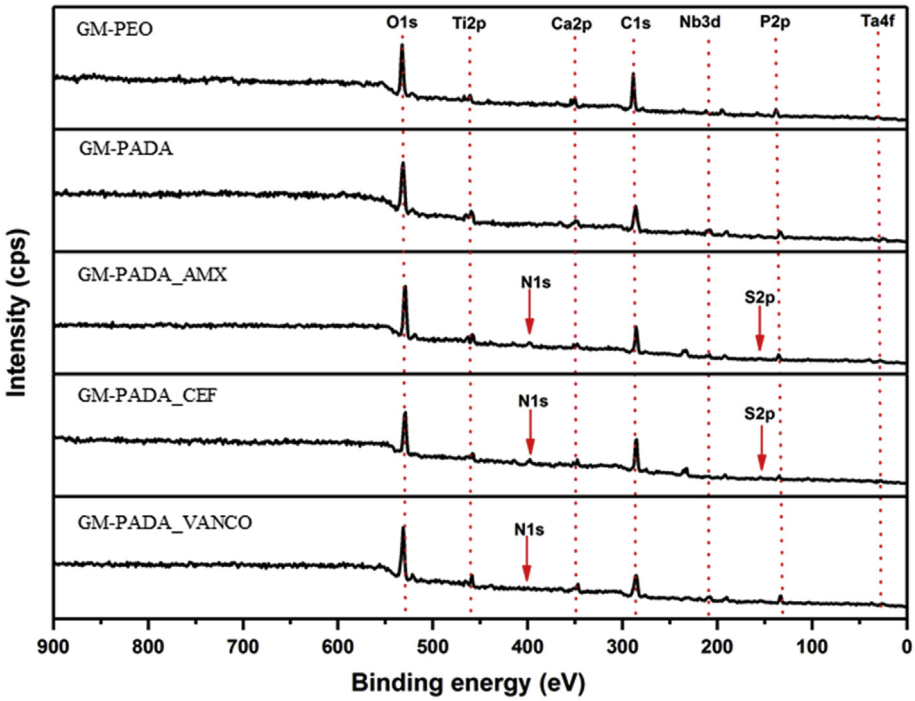

Fig. 4. XPS survey spectra recorded for the GM-PEO, GM-PADA, GM-PADA_AMX, GM-PADA_CEF and GM-PADA_VANCO samples.

significantly decreased. This tendency was also observed when the concentration of the drugs increased to 50 μg·mL^{-1}. For all drugs, their primary content in the PBS solution decreased after only 6.5 h of sample preparation. This meant that the drug concentration released from the coatings were determined with the error tolerance, which occurred due to the various stability of the drugs in the PBS solution. High drug concentrations in the PBS solution caused their stability to be much better, and the drugs were not adsorbed on the vial walls. Drug degradation products were not observed on all chromatograms. Based on these results, the drug concentrations released from the hybrid coatings was determined for up to 10 h after material immersion. This length of time is also the most important for preventing bacterial adhesion and biofilm formation.

Fig. 9 presents the results of the released drug concentration depending on the hybrid layer degradation time. For the GM-PADA_AMX sample after 0.5 h of hybrid layer degradation, the released amoxicillin concentration was 1.80 μg·mL^{-1}. Then, after 1 h of degradation, the drug concentration increased to 1.90 μg·mL^{-1} and after 2 h to 1.94 μg·mL^{-1}. Afterward, the concentration started to slightly decrease and was 1.51 μg·mL^{-1} after 4 h, 1.46 μg·mL^{-1} after 5 h, 1.48 μg·mL^{-1} after 6 h, 1.40 μg·mL^{-1} after 8 h and 1.38 μg·mL^{-1} after 10 h.

Contrary to the amoxicillin release from the GM-PADA_AMX

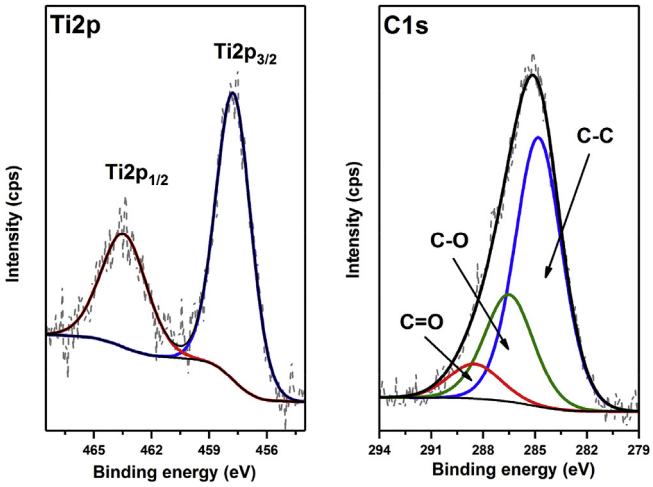

Fig. 6. High-resolution XPS spectra recorded for the GM-PADA sample: a) Ti 2p and b) C 1s.

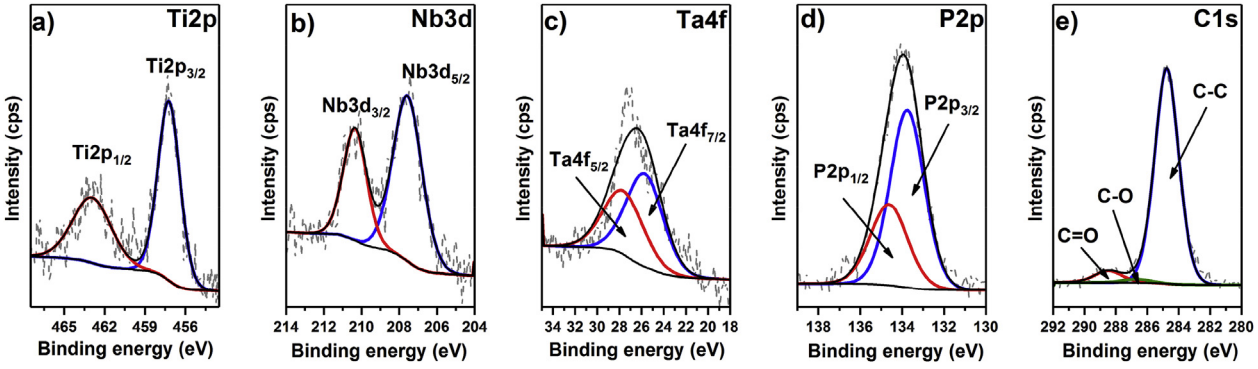

Fig. 5. High-resolution XPS spectra recorded for the GM-PEO sample: a) Ti 2p, b) Nb 3d, c) Ta 4f, d) P 2p and e) C 1s.

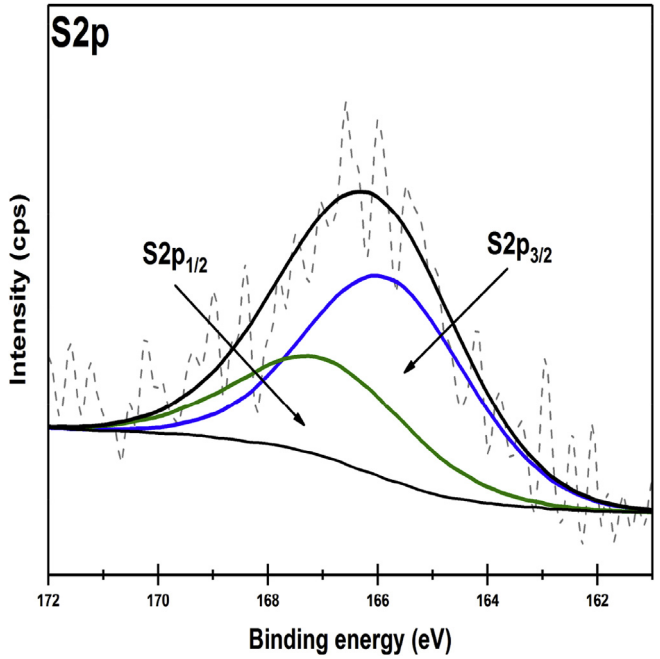

Fig. 7. High-resolution XPS spectra of the S 2p region recorded for the GM-PADA_AMX sample.

surface, the drug release concentration profile of cefazolin and vancomycin increased over time. The released cefazolin concentration started with 1.02 $\mu g \cdot mL^{-1}$ after 0.5 h and increased. It was 1.09 $\mu g \cdot mL^{-1}$ after 1 h, 1.15 $\mu g \cdot mL^{-1}$ after 2 h, 1.18 $\mu g \cdot mL^{-1}$ after 4 h and stayed the same after 5 h. The concentration was then 1.26 $\mu g \cdot mL^{-1}$ after 6 h, 1.33 $\mu g \cdot mL^{-1}$ after 8 h and 1.34 $\mu g \cdot mL^{-1}$ after 10 h.

Vancomycin was released with the highest concentrations. After 0.5, the released vancomycin concentration was 5.10 $\mu g \cdot mL^{-1}$. Then, the concentration was 5.48 $\mu g \cdot mL^{-1}$ after 1 h, 5.63 $\mu g \cdot mL^{-1}$ after 2 h, 5.43 $\mu g \cdot mL^{-1}$ after 4 h, 5.50 $\mu g \cdot mL^{-1}$ after 5 h, 5.78 $\mu g \cdot mL^{-1}$ after 8 h and 6.06 $\mu g \cdot mL^{-1}$ after 10 h.

3.5. Bacterial growth inhibition zones

Table 3 presents *Staphylococcus aureus* growth inhibition zones. For GM-PADA_AMX, the inhibition zone was measured and was 18 mm for an *S. aureus* clinical strain MRSA 1030, while it was larger, 30 mm, for the reference strain ATCC 25923. A different tendency was observed for GM-PADA_CEF and GM-PADA_VANCO, where growth inhibition zones of the reference *S. aureus* (ATCC 25923) were smaller than the clinical MRSA 1030 zones. The measurement values for GM-PADA_CEF were 24 mm (MRSA 1030) and 15 mm (ATCC 25923), and the measurement values for GM-PADA_VANCO were 16 mm (MRSA 1030) and 12 mm (ATCC 25923).

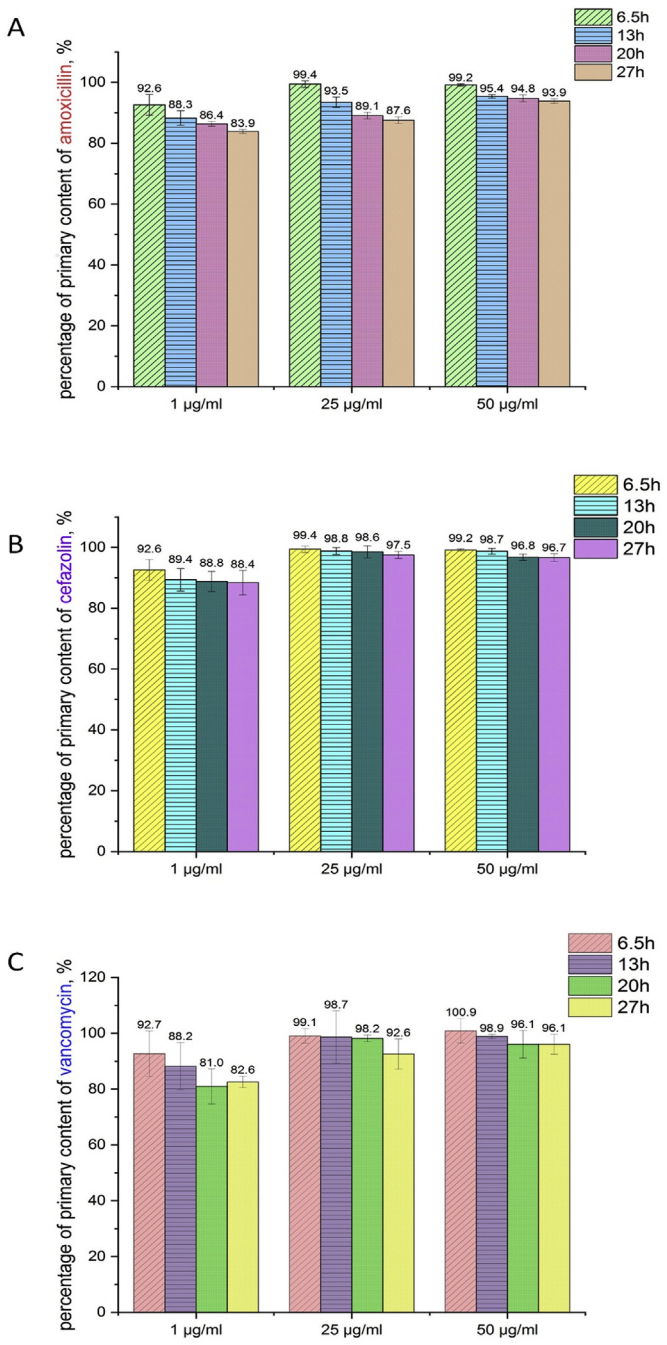

Fig. 8. Concentration of amoxicillin (A), cefazolin (B) and vancomycin (C) after different exposure times in PBS solution.

Table 2
Degradation of the polymer (PADA) and polymer with drugs: amoxicillin, cefazolin or vancomycin up to 48 h.

sample labels	calculated parameters	degradation time, h								
		1	2	4	6	8	10	12	24	48
PADA	anhydride groups/acid groups ratio [mol/mol]	1:0.31	1:0.47	1:0.88	1:1.08	1:1.68	1:1.74	1:1.59	1:3.57	1:7.29
	content of adipic acid [%]	**23.9**	**32.1**	**46.9**	**51.9**	**62.77**	**63.6**	**61.4**	**78.1**	**87.5**
PADA_AMX	anhydride groups/acid groups ratio [mol/mol]	1:0.55	1:0.74	1:1.23	1:1.77	1:1.62	1:1.52	1:1.62	1:4.22	1:9.08
	content of adipic acid [%]	**35.5**	**42.4**	**55.2**	**63.9**	**61.8**	**60.2**	**61.8**	**80.8**	**90.1**
PADA_CEF	anhydride groups/acid groups ratio [mol/mol]	1:0.97	1:1.19	1:2.00	1:2.12	1:1.95	1:2.28	1:2.13	1:6.28	1:7.92
	content of adipic acid [%]	**49.4**	**54.4**	**66.7**	**67.9**	**66.1**	**69.6**	**68.0**	**86.3**	**88.8**
PADA_VANCO	anhydride groups/acid groups ratio [mol/mol]	1:0.92	1:1.49	1:1.90	1:2.20	1:1.39	1:1.28	1:1.88	1:4.01	1:5.33
	content of adipic acid [%]	**47.8**	**59.9**	**65.5**	**68.7**	**58.2**	**56.1**	**65.3**	**80.0**	**84.2**

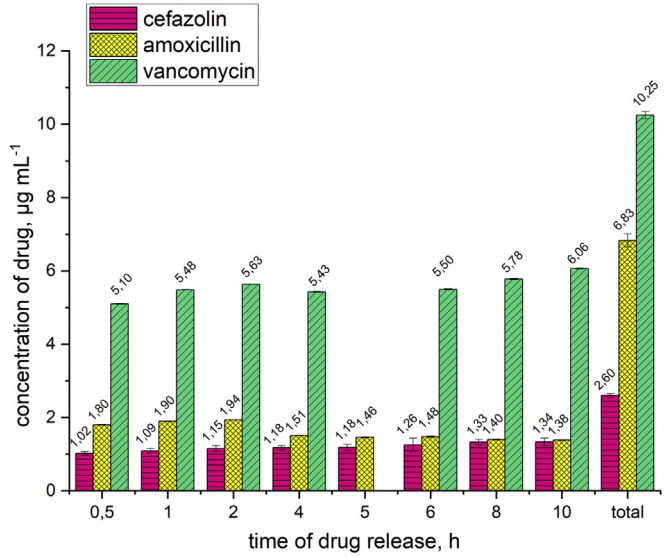

Fig. 9. Release concentrations of amoxicillin, cefazolin and vancomycin after hybrid layer degradation of up to 10 h.

Table 3
Clinical *Staphylococcus aureus* (MRSA 1030) and reference *Staphylococcus aureus* (ATCC 25923) growth inhibition zones.

sample	bacterial growth inhibition zone, mm	
	S. aureus (ATCC 25923)	*S. aureus* (MRSA 1030)
GM[a]	5	5
GM-PEO[a]	5	5
GM-PADA[a]	5	5
GM-PADA_AMX	30	18
GM-PADA_CEF	15	24
GM_PADA_VANCO	12	16

[a] Values of 5 mm indicate the collected solutions from the investigated places showed no inhibition zones.

3.6. Bacterial adhesion tests

The bacterial adhesion results are presented in Fig. 10. After comparing surfaces loaded with drugs to those without drugs, all drug-containing surfaces show a visible decrease in the amount of adhered bacteria. For the GM, GM-PEO and GM-PADA surfaces, the minimal observed adhered bacteria amount was $2.6{\cdot}10^{6}$ CFU·mL^{-1} (GM-PADA, ATCC 25923), and the maximal amount was $1.5{\cdot}10^{8}$ CFU·mL^{-1} (GM-PADA, MRSA 1030). Surfaces loaded with drug exhibited stronger bacteriostatic effects than those without antibiotics. The minimal amount of adhered bacteria was observed for the GM-PADA_CEF hybrid layer, which was equal to $1.5{\cdot}10^{5}$ CFU·mL^{-1} for the ATCC 25923 strain and $3.0{\cdot}10^{5}$ CFU·mL^{-1} for the MRSA 1030 strain. For the GM-PADA_AMX and GM-PADA_VANCO surfaces, the amount of *S. aureus*, in any case, was no higher than $4.1{\cdot}10^{6}$ CFU·mL^{-1} (GM-PADA_VANCO, ATCC 25923). It is worth noting that GM-PADA_CEF and GM-PADA_VANCO exhibited stronger antibacterial effects on the clinical strain (MRSA 1030) than on the reference strain (ATCC 25923). The amount of adhered bacteria was $2.3–4.8{\cdot}10^{9}$ CFU·mL^{-1} for the control measurement, and thus, all investigated samples revealed less favorable conditions for bacterial adhesion than the control.

3.7. Cytocompatibility

Fig. 11 presents the Alamar Blue percent reduction, which corresponds to the viability of MG-63 osteoblast-like cells on the investigated surfaces after incubation (24 h, 3 days and 7 days). The GM surface

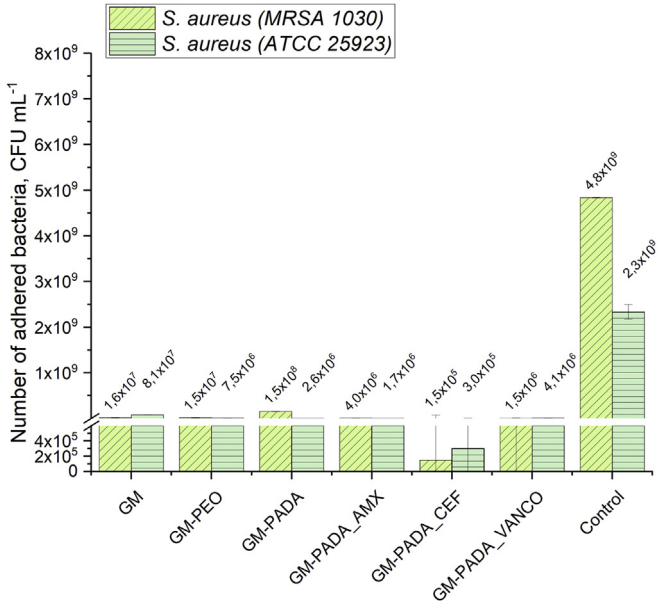

Fig. 10. Adhesion tests of *S. aureus* (ATCC 25923 and MRSA 1030) on investigated surfaces of GM, GM-PEO, GM-PADA, GM-PADA_AMX, GM-PADA_CEF and GM-PADA_VANCO.

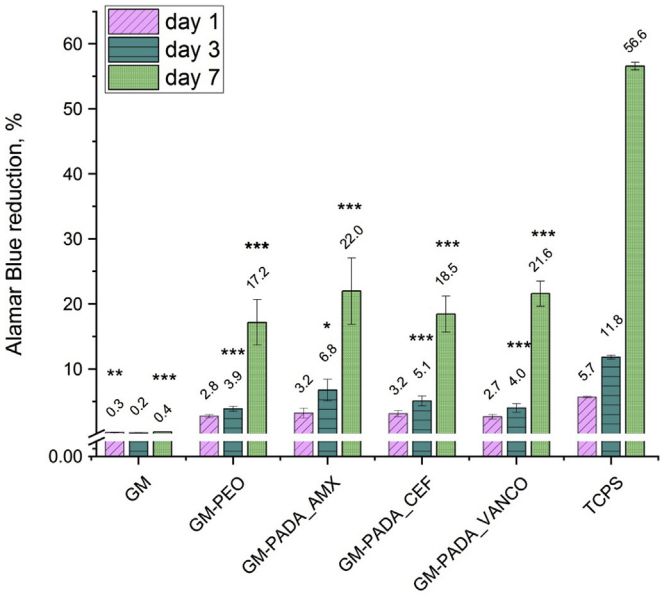

Fig. 11. Viability of MG-63 osteoblast-like cells after 24 h, 3 days and 7 days of incubation. The results are presented as the mean ± SD. Statistically significant differences between the samples and the control (TCPS) are indicated by * (* < 0.05, **p < 0.01, ***p < 0.001).

(unmodified Ti alloy surface) after the PEO treatment exhibited better cytocompatibility (GM-PEO sample). This can be related to the increase in roughness after the PEO process, but also the chemical composition of the oxide layer. The viability of the MG-63 cells on the hybrid layers was slightly higher than on the GM-PEO surface. After 7 days of incubation. 21.97% of Alamar Blue reduction was observed on the GM-PADA_AMX surface, while a similar result was observed for the GM-PADA_VANCO surface with a total of 21.58%. The GM-PADA_CEF surface exhibited a slightly lower Alamar Blue reduction percent than the above and was 18.46% after 7 days of incubation.

Fig. 12 presents images of the MG-63 cell cultures on the investigated surfaces. MG-63 cells on the GM surface were not well attached to the surface. The number of cells was rather small, and their

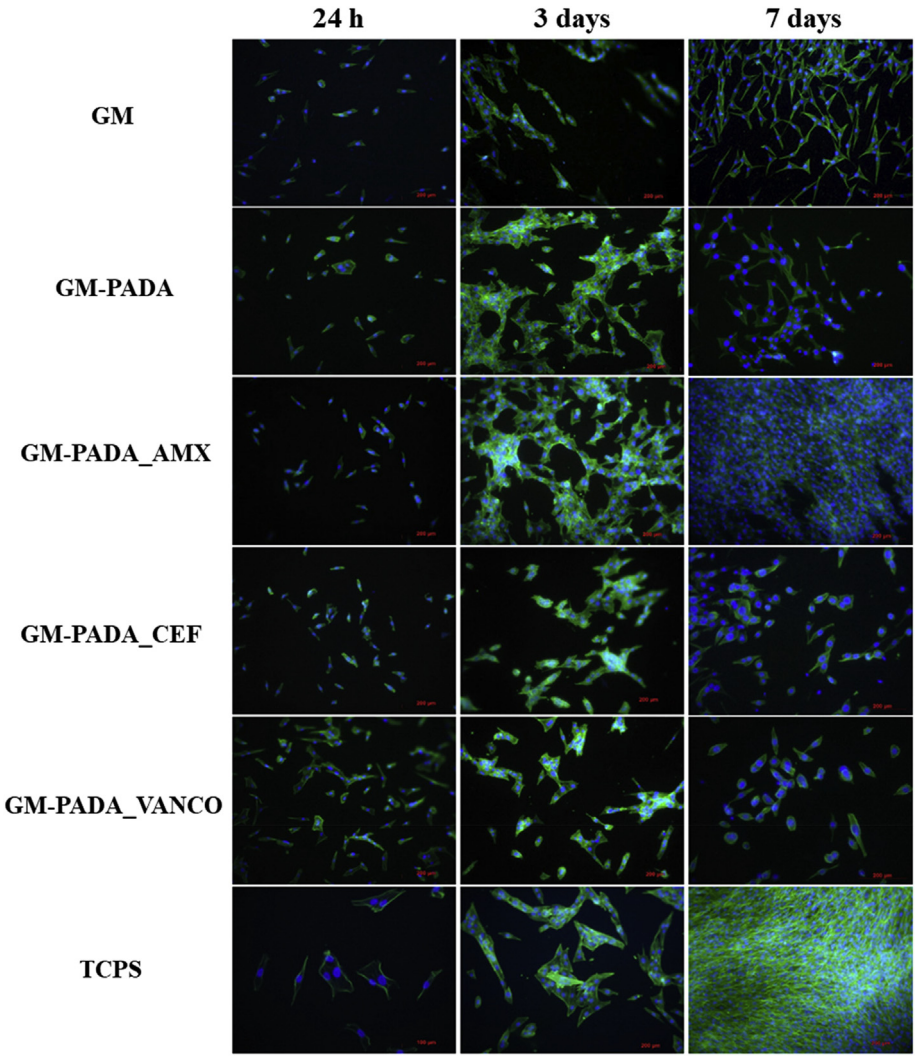

Fig. 12. MG-63 cell culture images after 24 h, 3 days and 7 days with the GM, GM-PADA, GM-PADA_AMX, GM-PADA_CEF and GM-PADA_VANCO surfaces and TCPS as a reference.

shape was triangular, which indicated a lack of cellular preference for proliferation on the GM surface. A completely different situation could be observed for the GM-PADA surface after PEO treatment and after polymer layer deposition. In this case, after 24 h, cells attached quite well on the surface, which could be observed due to their flatter shape and the increased number of cells. Comparing the GM-PADA surfaces with additions of amoxicillin, cefazolin or vancomycin, it could be seen that after 24 h of cell culture, the best results were obtained for the GM-PADA_VANCO surface, where the cells preferred adhesion and proliferation. The best results were observed for the 7-day MG-63 cell culture on the GM-PADA_AMX surface. Cells proliferated in the highest amount in comparison to other drug-loaded surfaces. For GM-PADA_CEF and GM-PADA_VANCO, the shape and amount of MG-63 cells was also evidence of good adhesion and proliferation of living cell conditions. All these results were also confirmed by cytocompatibility tests using the Alamar Blue reduction percentage.

4. Discussion

Among all biomaterials, titanium and its alloys seem to be favored for use as long-term implantable materials. This is not only due to the good mechanical and biocompatible properties or corrosion resistance of titanium but also the possibility of relatively simple surface treatment applications. Anodization of Ti alloy surfaces where spark discharges occur results in high porosity, increasing surface roughness and changing wettability, which are considered to be very important features for the integration of implant material with bone tissue. Additionally, adjusting the PEO parameters, such as applied voltage, current density or anodizing bath composition, provides an opportunity to create a variety of functional biomaterials with different surface characteristics. It has been reported that it is possible to anodize real-shape implants with a chemical composition suitable for their osseointegration process. The formation of hybrid coatings on real-shape implants is also possible. The dip-coating method is widely used, making it possible to cover the metal surface of complicated shapes. This advantage is technologically important for the successful surface treatment of Ti-based implants available on the market.

In this work, the results of the PEO treatment of the titanium alloy Ti–2Ta–3Zr–36Nb (GM sample) surface indicate that the wettability and surface roughness of the investigated samples increased. A slight increase in hydrophobicity was observed when comparing the contact angles of different GM-PADA surfaces to the GM-PEO surface, which can be explained by the hydrophobic structure of antibiotics loaded into the polymer layer or also changes of the surface roughness which significant influences on a wettability. However, every type of investigated surface revealed a contact angle of less than 90°, which confirms the hydrophilic character of the investigated materials. Additionally, the value of the arithmetic roughness coefficient increased after PEO and

was 1.53 μm–2.06 μm. Similar implant surface roughness and bone tissue can support osseointegration and long-term implant use. The required Ra value of implant-intended biomaterials should be approximately 2 μm [35].

The XPS surveys confirmed the presence of Ti_2O_3 in the oxide layer without breaking the continuity of the formed oxide layer. The incorporation of Calcium and phosphorus was also detected and verified. These elements are simultaneous bone building components, so their successful incorporation into the oxide layer increases its bioactivity. Polymer layer associations with the PEO layer were not observed via XPS analysis, which indicates that the degradation of the PADA layer can easily proceed in a human body fluid environment, enabling a controlled release of drugs. All these results prove PEO to be a good choice as a surface modification process because of the possibility of obtaining biomaterials with more biocompatible physicochemical properties when compared to bone tissue.

Septic bone inflammation is a common difficulty related to implantation processes. The main pathogen leading to this disease is the group of bacteria named *Staphylococcus* [36]. This kind of infection is very difficult to treat due to the ability of bacteria to create biofilms that are particularly resistant to different antibacterial agents [37]. According to MIC values presented in the available database EUCAST, the MIC of amoxicillin, cefazolin and vancomycin against *Staphylococcus aureus* and *Staphylococcus epidermidis* is in the range of 0.12 $\mu g \cdot cm^{-3}$ to 2.00 $\mu g \cdot cm^{-3}$. The results presented in this paper indicate a similar order of magnitude of bacteriostatic efficient concentrations of amoxicillin, cefazolin and vancomycin released from the hybrid layers. After 0.5 h of release, amoxicillin was released at a concentration of 1.8 $\mu g \cdot cm^{-3}$, cefazolin 1.02 $\mu g \cdot cm^{-3,}$ and for vancomycin was 5.10 $\mu g \cdot cm^{-3}$. Additionally, the bacterial growth inhibition zone measured for the solution containing antibiotics released from the hybrid layer after 0.5 h was in the range from 12 to 30 mm against *S. aureus* (ATCC 25923) and 16–24 against *S. aureus* (MRSA 1030). These results demonstrate the bacteriostatic effect of antibiotics containing PADA layers formed on GM surfaces against *Staphylococcus* bacteria after 0.5 h of release. The period of time immediately after the implantation process is especially important because of the treated tissues have an increased susceptibility to bacterial attack during surgery. The antibiotic release concentration did not change significantly after 10 h of hybrid layer degradation, revealing an undiminished release of antibiotic concentrations after 10 h.

The antibiotic stability was also determined. The results show that the stability of the investigated drugs was dependent on the initial drug concentration. Starting with drug concentrations equal to 25 $\mu g \cdot cm^{-3}$ or 50 $\mu g \cdot cm^{-3}$, the drug stability did not decrease below 87.6% (amoxicillin, 27 h). However, no degradation products of antibiotics were observed during HPLC, which suggests undiminished effectiveness of the drug released from the hybrid layer. Additionally, ^1H NMR studies show that PADA can be considered as a easily hydrolyzable polymer due to a higher than 85% of hydrolytic degradation. In conclusion, fast degradation of PADA can ensure sufficient antibiotic stability and, consequently, good antibacterial effectiveness of the formed hybrid layers.

All three investigated surfaces loaded with drugs (GM-PADA_AMX, GM-PADA_CEF and GM-PADA_VANCO) exhibited good cytocompatibility. According to tests with MG-63 osteoblast-like cells, there is a visible increase in cell proliferation after 7 days on every type of antibiotic-containing hybrid layer. Additionally, the images confirm good living cell proliferation conditions on the investigated surfaces. It is possible to observe that after 7 days of cell incubation, their amount and rather flat shape demonstrate good cytocompatibility with the investigated surfaces. Comparing these results to bacterial adhesion tests, it is worth noting that the PADA hybrid layers containing amoxicillin, cefazolin or vancomycin provide an opportunity to design biomaterials with good antibacterial and cytocompatible properties.

The coatings composed of cefazolin and vancomycin exhibited good cytocompatibillity, however the surface with cefazolin showed better properties against adhesion of the bacteria. These result is correlated with the drug concentration loaded into the polymer layer, where the concentration of cefazolin was higher than vancomycin. On the other hand, the molecular weight of vancomycin is much higher than for cefazolin, and the diffusion rate of drug into the solution could be significant different. Thus, the better activity against bacteria was observed for the sample with cefazolin, but concentration of drug loaded in both coatings (cefazolin and vancomycin) was not toxic for the MG-63 osteoblast cells. Fast degradation of PADA and, as a consequence, its fast antibiotic release can enable quick drug delivery directly to infected places, which claims to be a highly important feature of biomaterials designed as implants. It is also worth noting that bacterial growth inhibition zones for the GM-PADA_AMX of the clinical strain of *Staphylococcus aureus* (MRSA 1030) are significantly lower than in the case of the reference strain (ATCC 25923). Thus, the stronger antibacterial effect against the clinical *S. aureus* strain than against the reference strain can be concluded for the GM-PADA_AMX hybrid layer. It is also very beneficial because the clinical strains (for example, MRSA 1030) are generally more resistant to antibiotic action than the reference strains (ATCC 25923).

The coating formed by plasma electrolytic oxidation process, usually shows good adhesion to the substrate. It was reported, that the ceramic coating like TiO_2 formed on the Ti alloys during the anodization process, might be not brittle and not cracks during the scratch test measurements [38]. However, it should be point that the final effect depends on the anodization conditions and the structure of the formed coating. It was reported, that microstructure of the substrate strongly influences on the adhesion between a metal substrate and polymer layer [39]. In this case, the substrate is recognized as the anodized titanium alloy, which structure is favorable to attach polymer layer loaded with drug. It indicates, that the adhesion of the polymer on the top of the oxides could be satisfying. XPS analysis confirmed that there are no chemical connections between the polymer and the oxides, however the aim of this work is fast degradation of the polymer, so in this case is an advantage.

Titanium alloys called as gum metals, in this case Ti–2Ta–3Zr–36Nb, exhibit mechanical properties close to the natural bone. This is a promising material in implantology, due to the biocompatibility, excellent mechanical properties and possibility to make a real shape implants such as dental implants. However, price of the gum metals is relatively high at the moment, and the formation of the functional implant is expensive. On the other hand, this paper shows that the surface of this titanium alloys might be provided in easy way, and the results are promising to evaluate these implants (especially with amoxicillin) in *in vivo* experiments, according to the ISO 10993 standard.

5. Conclusions

In this paper, a poly(adipic anhydride) layer loaded with antibiotics was deposited on the surface of a Ti alloy, Ti–2Ta–3Zr–36Nb (type of Gum Metal), which was first treated using a plasma electrolytic oxidation process. The surface morphology, surface roughness and wettability for each of the obtained anodized surfaces were investigated. It was concluded that PEO surfaces were porous with an observable increase in surface roughness and wettability and demonstrated no observable defects or cracks. Next, for the Ti alloy oxide layer, the poly (adipic anhydride) containing one of three different drugs, amoxicillin, cefazolin or vancomycin, was deposited via a dip-coating method. The surface microstructure of the polymer was analyzed using a confocal microscope and indicated the specific microstructure, which was favorable for the adhesion and proliferation of MG-63 osteoblast-like cells MG-63. The obtained hybrid layer degradation time was measured up to 48 h, and poly(adipic anhydride) was concluded as a relatively fast-degrading polymer, achieving a hydrolysis progress of over 80% after

48 h of degradation. Furthermore, the XPS studies indicated that the poly(adipic anhydride) polymer was not associated with the Ti alloy oxide layer, allowing fast polymer degradation and drug release. The antibiotic release concentrations were measured up to 10 h, maintaining drug concentrations sufficient for inhibiting bacterial growth. The antibacterial effect of hybrid coatings was confirmed by tests with two bacterial strains: *Staphylococcus aureus* ATCC 25923 and *Staphylococcus aureus* MRSA 1030. Satisfactory results from the cytocompatibility studies using MG-63 osteoblast-like cells were also obtained. A good proliferation of living cells was determined on the investigated surfaces, even after the addition of antibiotics. The stability of released antibiotics was determined for up to 27 h, and after 6.5 h, the stability of the three drugs significantly decreased. These findings indicate that the evaluation of the drug release from the materials could not determine if 100% of the loaded drugs were effectively released.

CRediT authorship contribution statement

Katarzyna Leśniak-Ziółkowska: Investigation, Data curation. **Monika Śmiga-Matuszowicz:** Investigation. **Agata Blacha-Grzechnik:** Investigation, Visualization. **Sebastian Student:** Software. **Monika Brzychczy-Włoch:** Supervision. **Małgorzata Krok-Borkowicz:** Investigation. **Elżbieta Pamuła:** Supervision. **Wojciech Simka:** Supervision. **Alicja Kazek-Kęsik:** Conceptualization, Methodology, Software, Validation, Formal analysis, Investigation, Resources, Writing - original draft, Writing - review & editing, Visualization, Supervision, Project administration, Data curation.

Declaration of competing interest

Authors declare no conflict of interest.

Acknowledgments

This work was supported by the National Science Centre, Poland (UMO-2016/21/D/ST5/01652). This work was supported by Rector's Grant in the field of research and development (Silesian University of Technology, Poland, 04/010/RGJ19/0095).

The authors would like to thank Dr Joanna Płonka (Silesian University of Technology) for HPLC analysis.

Appendix A. Supplementary data

Supplementary data to this article can be found online at https://doi.org/10.1016/j.bioactmat.2020.04.020.

References

[1] G. Miranda, F. Sousa, M.M. Costa, F. Bartolomeu, F.S. Silva, O. Carvallo, Surface design using laser technology for Ti6Al4V-hydroxyapatite implants, Optic Laser. Technol. 109 (2019) 488–495, https://doi.org/10.1016/j.optlastec.2018.08.034.
[2] G. Miranda, F. Sousa, M.M. Costa, F. Bartolomeu, F.S. Silva, O. Carvallo, Surface design using laser technology for Ti6Al4V-hydroxyapatite implants, Optic Laser. Technol. 109 (2019) 488–495, https://doi.org/10.1016/j.optlastec.2018.08.034.
[3] N. Eliaz, Corrosion of metallic biomaterials: a review, Materials 12 (2019) 407–498, https://doi.org/10.3390/ma12030407.
[4] A. Krząkała, A. Kazek-Kęsik, W. Simka, Application of plasma electrolytic oxidation to bioactive surface formation on titanium and its alloys, RSC Adv. 3 (2013) 19725–19743, https://doi.org/10.1039/c3ra43465f.
[5] H. Krawiec, V. Vignal, J. Loch, P. Erazmus-Vignal, Influence of plastic deformation on the microstructure and corrosion behaviour of Ti–10Mo–4Zr and Ti– 6Al–4V alloys in the Ringer's solution at 37°C, Corrosion Sci. 96 (2015) 160–170, https://doi.org/10.1016/j.corsci.2015.04.006.
[6] D. Teker, F. Muhaffel, M. Menekse, N.G. Karaguler, M. Baydogan, H. Cimenoglu, Characteristics of multi-layer coating formed on commercially pure titanium for biomedical applications, Mater. Sci. Eng. 48 (2015) 579–585, https://doi.org/10.1016/j.msec.2014.12.058.
[7] D.M. Gordin, R. Ion, C. Vasilescu, S.I. Drob, A. Cimpean, T. Gloriant, Potentiality of the "Gum Metal" titanium-based alloy for biomedical applications, Mater. Sci. Eng. C 44 (2014) 362–370, https://doi.org/10.1016/j.msec.2014.08.003.
[8] T. Saito, T. Furuta, J. Hwang, S. Kuramoto, K. Nishino, N. Suzuki, R. Chen, Multifunctional alloys obtained via a dislocation-free plastic deformation mechanism, Science 300 (2003) 464–467, https://doi.org/10.1126/science.1081957.
[9] H. Chang, Y. Tseng, A novel β-titanium alloy orthodontic wire, Kaohsiung J. Med. Sci. 34 (2018) 202–206, https://doi.org/10.1016/j.kjms.2018.01.010.
[10] M. Mohedano, X. Lu, E. Matykina, C. Blawert, R. Arrabal, M.L. Zheludkevich, Plasma Electrolytic Oxidation (PEO) of Metals and Alloys, Encyclopedia of Interfacial Chemistry, Elsevier, Oxford, 2018, pp. 423–438, https://doi.org/10.1016/b978-0-12-409547-2.13398-0.
[11] P. Silva-Bermudez, S.E. Rodil, An overview of protein adsorption on metal oxide coatings for biomedical implants, Surf. Coating. Technol. 233 (2013) 147–158, https://doi.org/10.1016/j.surfcoat.2013.04.028.
[12] E. Matykina, R. Arrabal, M. Mohedano, A. Pardo, M.C. Merino, E. Rivero, Stability of plasma electrolytic oxidation coating on titanium in artificial saliva, J. Mater. Sci. Mater. Med. 24 (2013) 37–51, https://doi.org/10.1007/s10856-012-4787-z.
[13] P.L. Silva, J.D. Santos, F.J. Monteiro, J.C. Knowles, Adhesion and microstructural characterization of plasma-sprayed hydroxyapatite/glass ceramic coatings onto Ti-6A1-4V substrates, Surf. Coating. Technol. 102 (1998) 191–196, https://doi.org/10.1016/S0257-8972(97)00576-8.
[14] M.E. Olson, A.R. Hoswill, Staphylococcus aureus osteomyelitis: bad to the bone, Cell Host Microbe 13 (2013) 629–631, https://doi.org/10.1016/j.chom.2013.05.015.
[15] Y. Li, L. Liu, P. Wan, Z. Zhai, Z. Mao, Z. Ouyang, D. Yu, Q. Sun, L. Tan, L. Ren, Z. Zhu, Y. Hao, X. Qu, K. Yang, K. Dai, Biodegradable Mg-Cu alloy implants with antibacterial activity for the treatment of osteomyelitis: in vitro and in vivo evaluations, Biomaterials 106 (2016) 250–263, https://doi.org/10.1016/j.biomaterials.2016.08.031.
[16] W.J. Metsemakers, N. Emanuel, O. Cohen, N. Reichart, I. Potapova, T. Schmid, D. Segal, M. Riool, P.H.S. Kwakman, L. de Boer, A. de Breij, P.H. Nibbering, R.G. Richards, S.A.J. Zaat, F. Moriarty, A doxycycline-loaded polymer-lipid encapsulation matrix coating for the prevention of implant-related osteomyelitis due to doxycycline-resistant methicillin-resistant Staphylococcus aureus, J. Contr. Release 209 (2015) 47–56, https://doi.org/10.1016/j.jconrel.2015.04.022.
[17] D.P. Lew, F.A. Waldvogel, Osteomyelitis Lancet 364 (2004) 369–379, https://doi.org/10.1016/S0140-6736(04)16727-52.
[18] R.O. Darouiche, Treatment of infections associated with surgical implants, N. Engl. J. Med. 350 (2004) 1422–1429, https://doi.org/10.1056/NEJMra035415.
[19] European committee on antimicrobial susceptibility testing – EUCAST, http://www.eucast.org/ accessed 08.01.2020.
[20] L.W. Kleiner, J.C. Wright, Y. Wang, Evolution of implantable and insertable drug delivery systems, J. Contr. Release 181 (2014) 1–10, https://doi.org/10.1016/j.jconrel.2014.02.006.
[21] Y.J. Li, C.C. Lu, W.L. Tsai, M.H. Tai, An intra-oral drug delivery system design for painless, long-term and continuous drug release, Sensor. Actuator. B Chem. 227 (2016) 573–582, https://doi.org/10.1016/j.snb.2015.12.081.
[22] W. Ji, F. Yang, H. Seyednejad, Z. Chen, W.E. Hennink, J.M. Anderson, J.J.J.P. van den Beucken, J.A. Jansen, Biocompatibility and degradation characteristics of PLGA-based electrospun nanofibrous scaffolds with nanoapatite incorporation, Biomaterials 33 (2012) 6604–6614, https://doi.org/10.1016/j.biomaterials.2012.06.018.
[23] P.L.H. Lai, C.C. Liu, H.H. Tsang, C.D. Wei, H.C. Lih, W.J. Chu, I. Ming, Mixed micelles from methoxy poly(ethylene glycol)-polylactide and methoxy poly(ethylene glycol)-poly(sebacic anhydride) copolymers as drug carriers, React. Funct. Polym. 72 (2012) 846–855, https://doi.org/10.1016/j.reactfunctpolym.2012.07.014.
[24] K.A. Athanasiou, C.M. Agrawal, F.A. Barber, S.S. Burkhart, Orthopaedic applications for PLA-PGA biodegradable polymers, Arthrosc. J. Arthrosc. Relat. Surg. 14 (1998) 726–737, https://doi.org/10.1016/S0749-8063(98)70099-4.
[25] A. Kazek-Kęsik, J. Jaworska, M. Krok-Borkowicz, M. Gołda-Cępa, M. Pastusiak, M. Brzychczy-Włoch, E. Pamuła, A. Kotarba, W. Simka, Hybrid oxide-polymer layer formed on Ti-15Mo alloy surface enhancing antibacterial and osseointegration functions, Surf. Coating. Technol. 302 (2016) 158–165, https://doi.org/10.1016/j.surfcoat.2016.05.073.
[26] K. Jelonek, J. Kasperczyk, S. Li, P. Dobrzynski, B. Jarzabek, Controlled poly(l-lactide-co-trimethylene carbonate) delivery system of cyclosporine a and rapamycine – the effect of copolymer chain microstructure on drug release rate, Int. J. Pharm. 414 (2011) 203–209, https://doi.org/10.1016/j.ijpharm.2011.05.035.
[27] A.J. Alanis, Resistance to antibiotics: are we in the post-antibiotic era? Arch. Med. Res. 36 (2005) 697–705, https://doi.org/10.1016/j.arcmed.2005.06.009.
[28] A.C. Albertsson, M. Eklund, Influence of molecular structure on the degradation mechanism of degradable polymers: in vitro degradation of poly(trimethylene carbonate), poly(trimethylene carbonate-co-caprolactone), and poly(adipic anhydride), J. Appl. Polym. Sci. 57 (1995) 87–103, https://doi.org/10.1002/app.1995.070570109.
[29] I. Fogelberg, U. Edlund, B.O. Lundgren, A.C. Albertsson, S.K. Singh, Sterilization, storage stability and in vivo biocompatibility of poly(trimethylene carbonate)/poly (adipic anhydride) blends, Biomaterials 21 (2002) 945–955, https://doi.org/10.1016/s0142-9612(99)00268-9.
[30] A.C. Albertsson, J. Carlfors, C. Sturesson, Preparation and characterisation of poly (adipic anhydride) microspheres for ocular drug delivery, J. Appl. Polym. Sci. 62 (2002) 695–705, https://doi.org/10.1002/(sici)1097-4628(19961024)62:4<695::aid-app13>3.3.co;2-4.
[31] G.L. Kennedy, Toxicity of adipic acid, Drug Chem. Toxicol. 25 (2002) 191–202, https://doi.org/10.1081/DCT-120003259.
[32] S. Amselem, A. Domb, M. Maniar, J. Shah, Polyanhydrides – synthesis and characterization, Adv. Polym. Sci. 107 (1993) 93–141, https://doi.org/10.1007/BFb0027552.
[33] A. Kazek-Kęsik, G. Dercz, I. Kalemba, J. Michalska, J. Piotrowski, W. Simka, Surface

treatment of a Ti6Al7Nb alloy by plasma electrolytic oxidation in a TCP suspension, Arch. Civ. Mech. Eng. 14 (2014) 671–681, https://doi.org/10.1016/j.acme.2013.10.008.
[34] K. Leśniak, J. Płonka, M. Śmiga-Matuszowicz, M. Brzychczy-Włoch, A. Kazek-Kęsik, Functionalization of PEO layer formed on Ti-15Mo for biomedical application, J. Biomed. Mater. Res. (2019) 1–12, https://doi.org/10.1002/jbm.b.34504.
[35] A. Wennerberg, T. Albrektsson, Implant surfaces beyond micron roughness. Experimental and clinical knowledge of surface topography and surface chemistry, Int. Dent. 8 (2006) 14–16.
[36] M. Ribeiro, F.J. Monteiro, M.P. Ferraz, Infection of orthopedic implants with emphasis on bacterial adhesion process and techniques used in studying bacterial-material interactions, Biomatter 2 (2012) 176–194, https://doi.org/10.4161/biom.22905.
[37] L.G. Harris, R.G. Richards, Staphylococci and implant surfaces: a review, Inj. Int. J. Care Inj. 37 (2006) 3–14, https://doi.org/10.1016/j.injury.2006.04.003.
[38] E. Santos Jr., G.B. de Souza, F.C. Serbena, H.L. Santos, G.G. de Lima, E.M. Szesz, C.M. Lepienski, N.K. Kuromoto, Effect of anodizing time on the mechanical properties of porous titania coatings formed by micro-arc oxidation, Surf. Coating. Technol. 309 (2017) 203–211, https://doi.org/10.1016/j.surfcoat.2016.11.063.
[39] T. Kleffel, D. Drummer, Investigating the suitability of roughness parameters to assess the bond strength of polymer-metal hybrid structures with mechanical adhesion, Composites Part B 117 (2017) 20–25, https://doi.org/10.1016/j.compositesb.2017.02.042.